JOURNAL OF PROPULSION AND POWER
Vol. 11, No. 5, September–October 1995

Flow Instability in Plane–Parallel Particle Beds with Constant Volumetric Heating

J. L. Kerrebrock* and J. Kalamas†
Massachusetts Institute of Technology, Cambridge, Massachusetts 02139

This article addresses one possible form of instability in particle-bed nuclear reactors. One of the unresolved questions about this concept is whether the flow through the particle bed will be well-behaved, or will be subject to destructive flow instabilities. These may be of several types, some connected to the annular geometry, some to the nucleonics. This article addresses instabilities due to the heat addition process in the particle bed. A general three-dimensional model of the bed is adopted here, in which the fluid has mobility in three dimensions. From the sample calculations, which have been carried out for plane–parallel bed geometry, it could be concluded that a particle bed without a cold frit would be subject to instability if operated at the high-temperature ratios desired for nuclear rockets, and at power densities below about 4 MW/l. Since the desired power density is about 40 MW/l, operation at design exit temperature but at reduced power could be hazardous for such a reactor. The plane–parallel calculations show that appropriate combinations of cold and hot frits may cure such instabilities, but extension of the analysis to the annular geometry preferred for reactors has indicated that their stabilizing effect is much weaker in this geometry. More definite conclusions must await calculations for specific designs.

Introduction

THE nuclear rocket holds great potential for space missions requiring velocity increments that are at the limits of or beyond the capabilities of single-stage chemical rockets. Among these, the exploration of Mars by humans is the most prominent. Because of the large masses required for such missions, the factor of 2 reduction in mass in low Earth orbit (LEO), which the nuclear rocket promises by virtue of its high specific impulse, is very attractive. Such gains can be realized by use of the NERVA class technologies developed in the late 1960s and early 1970s. The NERVA reactors used cores in which the fuel elements were long hexagonal graphite cylinders with multiple circular cooling passages, the hydrogen propellant passing from the cold inlet end of the reactor through the passages to the hot exit end adjacent to the nozzle. The flow configuration thus consisted of a series of parallel passages of high length-to-diameter ratio. While conceptually appealing, this geometry poses problems in the mechanical support of the hot end of the core with allowance for thermal expansion. Furthermore, conduction of the heat from the interior of the fuel elements to the cooling passages sets limits on the power density and resultant power-to-weight ratio.

The particle-bed core offers mitigation of some of these limitations. Dividing the fuel elements into small spherical particles contained in a cylindrical bed through which the propellant flows radially may reduce the thermal stress in the fuel elements, allowing higher propellant temperatures to be reached. The high-temperature regions of the reactor are confined to the interior of cylindrical fuel assemblies, so that the major portion of the reactor can be relatively cool. This enables the use of structural and moderating materials other than graphite, reducing the minimum critical size of the reactor. The distinction between particles as referred to here and pebbles as referred to in some reactor contexts, is in the size of the individual fuel elements, particles being on the order of 1 mm in diameter, while pebbles are on the order of 1 cm or larger.

One of the unresolved questions about this concept is whether the flow through the particle bed will be well-behaved or will be subject to destructive instabilities of various types. Among the possibilities are maldistributions of flow due to the annular geometry with axial exhaust, interactions of the fuel bed density with the nucleonics, and others. This article considers instabilities associated with the heat addition in the particle bed. Intuitively, such instabilities may be expected if heat addition to the propellant flowing through the particle bed results in increased pressure drop, which may tend to reduce the flow. The heat generation being fixed by the nuclear processes, the reduced flow could result in increased temperature rise, more pressure drop and further reduced flow, and so it is possible that a runaway situation could develop. The possibility of such an instability is decreased by the normal viscous and turbulent pressure drops in the bed that tend to distribute the flow uniformly, so that the question of instability devolves to whether there is a mechanism by which heat addition can increase the pressure drop. One possible mechanism lies in the increase of fluid viscosity with temperature. This has been shown to lead to "laminar flow instability" at low Reynolds numbers when the fluid is constrained to passages, as in the NERVA cores. Such an instability was analyzed by Bussard and Delauer[1,2] in the context of NERVA-type nuclear rockets and has been treated by others for other applications.[3,4]

Most of the recent analyses of this type of instability of the particle bed reactor[5,6] have been extensions of the approach of Bussard and Delauer, where the bed is essentially treated as an array of parallel passages, so that the mass flow is continuous from inlet to outlet through any one passage. This approach will here be termed the parallel-stream model. A more general three-dimensional model of the bed is adopted here, in which the fluid has mobility in three dimensions rather than being constrained to flow in solenoidal fashion as if in a series of parallel passages. This three-dimensional stability problem will be approached at several increasingly sophisti-

Presented as Paper 93-1758 at the AIAA/SAE/ASME/ASEE 29th Joint Propulsion Conference and Exhibit, Monterey, CA, June 28–30, 1993; received Nov. 19, 1993; revision received June 23, 1994; accepted for publication Nov. 16, 1994.

*R. C. Maclaurin Professor of Aeronautics and Astronautics. Fellow AIAA.

†Research Assistant, Department of Aeronautics and Astronautics.

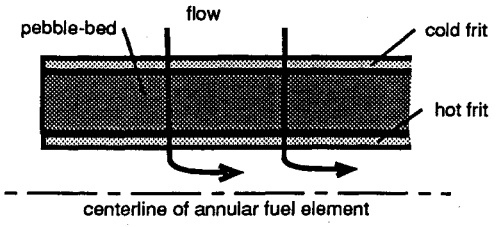

Fig. 1 Schematic of the particle bed.

cated levels, beginning with the parallel-stream model, which is essentially equivalent to the Bussard and Delauer approach.

Modeling

The particle-bed reactor is modeled for the present purpose as a plane–parallel bed of particles, which produce heat at a volumetric power Q, between two layers of porous media that represent the frits that control the inflow of fluid, and also contain the particles.

This model is shown schematically in Fig. 1.

In the steady state, all flow properties are functions only of x, the coordinate perpendicular to the plane of the bed. The fluid, a gas in this case, enters the particle bed through one porous region, termed the "cold frit," is heated in the particle bed, then leaves through the second porous region, the "hot frit."

For the nuclear rocket application, there will typically be a large fractional change in temperature through the bed, such that the fluid temperature at exit is five times or more the temperature at entrance to the bed. We characterize this rise by the ratio of the temperature difference across the bed, to the entrance temperature, the ratio being denoted q.

There is also a pressure drop through the bed due to both viscous and turbulent losses in the bed, and to the flow acceleration. Typically, the fractional pressure drop is 10% or less, and the viscous and turbulent losses dominate the flow acceleration.

It will be assumed for this analysis that the volumetric power Q is constant in space and in time. In fact, the heat release per unit of mass of nuclear fuel is governed principally by the local neutron flux, so that Q could vary in time and space with the flux. Since the neutron flux is not strongly coupled to the local fluid flow condition, it seems appropriate to consider Q independent of time. Spatial variations of Q through the bed may result from variations of either the neutron flux or the fuel concentration, but these are specific to the geometric details of the actual reactor. It seems consistent with the idealization to a plane–parallel geometry, to take Q constant in x.

There is a possible secondary coupling of Q to the fluid behavior, through a temperature dependence of the fission cross reaction. Both U^{235} and Pu^{239} fission cross reactions have some dependence on the (thermal) neutron temperature. But since we are assuming the neutrons are not locally coupled to the fluid properties, it is consistent to neglect this effect.

General Formulation

The authors have carried out independent analyses of the instability process, to guard against algebraic and computational errors. The formulation of the first author differs from that of the second author in only one way physically, through the inclusion of fluid acceleration terms in the fluid momentum equation by the latter. The formulation and the numerical results given here are those of the first author, except for some showing the effect of a hot frit and some showing the effect of annular geometry, that were obtained by the second author. As we shall see, the two independent calculations are in agreement where they overlap, confirming the absence of errors.

The flow velocity in the bed, $\boldsymbol{u}$, will be related to the pressure distribution by an Ergun[7] type relation

$$\nabla p = -\frac{\mu}{k}\boldsymbol{u} - \frac{b}{k}|\boldsymbol{u}|\rho\boldsymbol{u} \tag{1}$$

where the first term represents the laminar viscous contribution to the pressure gradient, and the second term represents the turbulent pressure gradient. The constant k depends on the porosity of the bed, as does b. According to Charmchi et al.,[5] for the bed of spheres with diameter D_p and void fraction ε

$$\frac{\mu}{k} = 150\frac{(1-\varepsilon)^2}{\varepsilon^3}\frac{\mu(T_g)}{D_p^2}$$
$$\frac{b}{k} = 1.75\frac{(1-\varepsilon)}{\varepsilon^3}\frac{1}{D_p} \tag{2}$$

It should be clear that the overall fluid acceleration

$$\rho(D\boldsymbol{u}/Dt) = \rho\left(\frac{\partial \boldsymbol{u}}{\partial t} + \boldsymbol{u}\cdot\nabla\boldsymbol{u}\right)$$

is neglected in this formulation. This is appropriate to the present physical situation of diffusive, low Reynolds number flow. The energy balance for the bed will be formulated in terms of separate relations governing the particle and g temperatures. It will later be shown that, in fact, the two temperatures are nearly coincident for many circumstances, but this will not be assumed at the outset. For the particle temperature T_p

$$\rho_s c_{ps}\frac{\partial T_p}{\partial t} = Q - \rho u c_p(T_p - T_g)h + k_{\text{eff}}\nabla^2 T_p \tag{3}$$

where ρ_s is the density of particles in the bed, c_{ps} is the corresponding specific heat, while c_p is the specific heat of the gas. Q is the power per unit volume, and k_{eff} is a heat transfer coefficient. Conduction and radiative heat transport in the bed are represented by the last term.

Here, we represent k_{eff} by

$$k_{\text{eff}} = k_{\text{cond}} + k_{\text{rad}} = k_{\text{cond}} + \tfrac{16}{3}\sigma D_p T_p^3 \tag{4}$$

the form of k_{rad} indicated by the last term is that given by Zeldovich and Raizer.[8]

Consistent with the pressure gradient formulation of Eq. (1), we assume a heat transfer coefficient with both laminar and turbulent contributions

$$h = (d/2kD_p)[(D_p/Re) + b]$$

where d is a hydraulic diameter for the flow passages between the particles, which we take as $d = \varepsilon D_p$. Then with Eq. (2)

$$h = \frac{75}{D_p}\frac{(1-\varepsilon)^2}{\varepsilon^2}\frac{1}{Re} + \frac{0.875}{D_p}\frac{(1-\varepsilon)}{\varepsilon^2} \tag{5}$$

The magnitude of k_{cond} is difficult to estimate, as it depends on contact between the particles and the gaseous conduction in the interstices. It will be treated parametrically, as a fraction of the conductivity of the particle material.

The energy balance for the gas is

$$\rho c_p\frac{\partial T_g}{\partial t} + \rho\boldsymbol{u}\cdot\nabla c_p T_g = \rho u c_p(T_p - T_g)h \tag{6}$$

Here, conduction in the gas is neglected, relative to conduction in the particles.

The formulation is completed by the statement of conservation of mass and the equation of state for the gas:

$$\frac{\partial \rho}{\partial t} + \nabla \cdot (\rho \boldsymbol{u}) = 0 \tag{7}$$

$$p = \rho R T \tag{8}$$

For convenience in the subsequent analysis, all quantities will be nondimensionalized, lengths by the depth l of the bed, and flow properties by their values $p_0(0)$, $\rho_0(0)$, $T_0(0)$, $u_0(0)$ at the entrance to the packed bed.

Then Eq. (1) becomes

$$\nabla p = -b_1 T_g^{\nu} \boldsymbol{u} - b_2 |\boldsymbol{u}| \rho \boldsymbol{u} \tag{1a}$$

where

$$b_1 = \frac{\mu_0(0) u_0(0) l}{p_0(0) k}$$

$$b_2 = \frac{b \rho_0(0) u_0^2(0) l}{p_0(0) k}$$

and the viscosity has been assumed to be of the form

$$\mu(T_g) = \mu_0(0) \left[\frac{T_g}{T_g(0)} \right]^{\nu}$$

Similarly, Eq. (3) is

$$c \frac{\partial T_p}{\partial t} = q - \rho u (T_p - T_g) H + K \nabla^2 T_p \tag{3a}$$

where

$$c \equiv \frac{\rho_s c_{ps}}{\rho_0(0) c_p}, \qquad H \equiv hl$$

$$K \equiv \frac{k_{\text{eff}}}{p_0(0) u_0(0) c_p l} \equiv K_c + K_r T_p^3$$

$$q \equiv \frac{Ql}{\rho_0(0) u_0(0) c_p T_0(0)}$$

Equation (6) becomes

$$\rho \frac{\partial T_g}{\partial t} + \rho \boldsymbol{u} \cdot \nabla T_g = \rho u (T_p - T_g) H \tag{6a}$$

Finally, Eqs. (7) and (8) become

$$\frac{\partial \rho}{\partial t} + \nabla \cdot \rho \boldsymbol{u} = 0 \tag{7a}$$

$$p = \rho T_g \tag{8a}$$

Zeroth Order or Steady Solution

Adding Eqs. (3a) and (6a) for the steady case yields

$$\rho_0 u_0 \frac{dT_{g0}}{dx} = q + K \frac{d^2 T_p}{dx^2}$$

Since for this case (7a) gives $\rho_0 u_0 = 1$, the simplest solution is

$$T_{g0} = 1 + qx \tag{9}$$

and from (3a) a consistent solution for T_p is

$$T_{p0} = 1 + qx + (q/H) \tag{10}$$

There are other solutions of the steady state, for which $d^2 T_{p0}/dx^2$ is nonzero, and these could be required if boundary conditions are prescribed on T_p, but for the present purpose the simpler situation will serve as the zeroth order. It should be noted, however, that the solution we have adopted implies heat conduction from the bed at the inflow boundary, and into it at the outflow boundary. It is unlikely that this has much influence on the flow stability.

With the dependence (9) for T_{g0}, Eq. (1a) becomes

$$p_0 \frac{dp_0}{dx} = -b_1 (1 + qx)^{\nu+1} - b_2 (1 + qx)$$

or upon integration

$$p_0^2 = 1 - \frac{2b_1}{(\nu + 2)q} [(1 + qx)^{\nu+2} - 1] - \frac{b_2}{q} [(1 + qx)^2 - 1] \tag{11}$$

The remaining flow variables are then determined to zeroth order by

$$\rho_0 = p_0 / T_{g0} \tag{12}$$

$$u_0 = 1/\rho_0 \tag{13}$$

First Order

Denoting the first-order, or fluctuating quantities by symbols without subscripts to distinguish them from the zeroth-order quantities denoted by the subscript 0, Eq. (1a) is to first-order

$$\nabla p = -b_1 [T_{g0}^{\nu} \boldsymbol{u} + i u_0 \nu T_{g0}^{\nu-1} T_g] - b_2 [\boldsymbol{u} + \boldsymbol{i}(u_0^2 \rho + u_x)] \tag{14}$$

where $\boldsymbol{i}$ is the unit vector in x.

Similarly, (3a) and (6a) yield

$$c \frac{\partial T_p}{\partial t} = -H(T_p - T_g) - H(T_{p0} - T_{g0})(\rho_0 u_x + u_0 \rho) + K \nabla^2 T_p \tag{15}$$

$$\rho_0 \frac{\partial T_g}{\partial t} + \rho_0 \frac{dT_{g0}}{dx} u_x + u_0 \frac{dT_{g0}}{dx} \rho + \frac{\partial T_g}{\partial x} = \rho_0 (T_{p0} - T_{g0}) H u_x + u_0 (T_{p0} - T_{g0}) H \rho + H(T_p - T_g) \tag{16}$$

Finally, Eqs. (7a) and (8a) yield

$$\frac{\partial \rho}{\partial t} + \rho_0 \nabla \cdot \boldsymbol{u} + \frac{d\rho_0}{dx} u_x + u_0 \frac{\partial \rho}{\partial x} + \frac{du_0}{dx} \rho = 0 \tag{17}$$

$$p = \rho_0 T_g + T_{g0} \rho \tag{18}$$

Here, the variables are to be regarded as p, ρ, T_g, $\boldsymbol{u}$, and T_p, so that they are seven.

Approaches to Analysis of Stability

It should be apparent from Eqs. (14–18) that a comprehensive analysis of the stability of the flow in the packed bed bounded by two frits can be complex. There are two levels of approach to the overall stability issue that have been used, and will be discussed here. These are 1) a parallel flow in-

stability and 2) a full three-dimensional instability analyzed with account for inflow and outflow boundary values and for the zeroth-order variation within the bed.

A brief delineation of these approaches will be offered here, before proceeding with the details of each.

Parallel-Flow Instability

The stability of the particle-bed reactor has conventionally been analyzed in this approximation, where the flow through the bed is modeled by parallel streams, generally without mass flow exchange between the streams.[5,6] This approach is analogous to that used by Bussard and DeLauer in analysis of the stability of NERVA-type nuclear rockets.[1,2] They found that such cases would be unstable to mass exchange between parallel cooling passages under low Reynolds number conditions where the increase of laminar viscosity with temperature became controlling, so that the pressure drop in a channel could increase with reduced mass flow.

This class of instability can be analyzed within the framework presented here, by calculating the pressure drop through the bed, from the zeroth-order solution [Eq. (11)]. If the pressure drop decreases with increasing flow, for constant volumetric heat addition, this is an indication of possible instability.

It is not a firm criterion, however, because, in fact, the flow can distribute laterally in the bed, an effect that is included in the more complete model.

Full Stability Analysis

Here, the disturbance is treated as harmonic in distance parallel to the plane of the bed and exponential in time, and so Eqs. (14–18) yield a system of ordinary differential equations in x, but with variable coefficients. Since they admit of no standard solutions, the eigenvalues representing growth rate must be found by numerical solution of the two-point boundary value problem. It is difficult to ensure that the most unstable solutions have in fact been identified, but in the view of the author this is the most reliable approach to the stability problem.

Parameters

The full set of dimensionless parameters required to specify Eqs. (1a–8a) is

from (1a)

$$v,\ b_1,\ b_2$$

from (3a)

$$q,\ c,\ H,\ K_c,\ K_r$$

Of these, v, K_c, and K_r are determined by the physical characteristics of the particle bed and propellant. The remainder are determined in part by the bed and in part by the operating conditions of the particle-bed reactor. To reduce this large set of parameters to a manageable and intuitively comprehensible set, typical values will be assigned to the physical characteristics of the bed, and the dimensionless variables will then be interpreted in terms of the operating variables, in ranges typical of those proposed for the particle-bed nuclear rocket.

There are three principal and independently assignable operating parameters for such rockets. They are the propellant exit pressure and temperature, and the power density (but as will be explained later these three are related for a device of given geometry, by exit-nozzle-flow choking). Nominal values of these proposed for the particle-bed reactor are

$$\begin{aligned} T_{g0}(\text{exit}) &= 3000\ \text{K} \\ p_0(\text{exit}) &= 100\ \text{atm} \\ Q &= 4 \times 10^{10}\ \text{W/m}^3 \end{aligned}$$

The proposed designs use bed depths of about 1 cm and particle diameters of 0.5 mm, and so we will use these as typical:

$$\begin{aligned} l &= 0.01\ \text{m} \\ D_p &= 0.5 \times 10^{-3}\ \text{m} \end{aligned}$$

Hydrogen is the propellant of choice, with a viscosity at 300 K of

$$\mu(300) = 0.87 \times 10^{-5}\ \text{kg/sm}$$

and for the temperature range 300–3000 K, a good approximation is

$$\nu = 0.70$$

In the use of the parallel-flow stability criterion it has become usual to present the stability as a boundary on coordinates of q vs Re, based on inflow fluid properties and D_p, and this practice will be followed here. In terms of q, Q, and other properties, we have

$$Re = \frac{\rho_0(0)u_0(0)D_p}{\mu(0)} = \frac{D_pQl}{c_pT_0\mu(0)_q} \tag{19}$$

the definition of q having been used in the second equality. Thus, for specified bed properties, inlet temperature and dimensionless temperature rise q, Re may be regarded as a surrogate for the power density Q.

The remaining dimensionless parameters can be evaluated in terms of these and the bed properties. Thus,

$$\begin{aligned} b_1 &= \frac{150(1-\varepsilon)^2}{\varepsilon^3}\frac{1}{D_p}\frac{\gamma M_0^2(0)}{Re} \\ b_2 &= 1.75\frac{(1-\varepsilon)}{\varepsilon^3}\frac{1}{D_p}\gamma M_0^2(0) \end{aligned} \tag{20}$$

where $M_0(0)$ is the flow Mach number at inlet and is given by

$$M_0(0) = \frac{\gamma - 1}{\gamma}\frac{Ql}{p_0(0)q\sqrt{\gamma RT_0(0)}} \tag{21}$$

Similarly,

$$H = 75\frac{l}{D_p}\frac{(1-\varepsilon)^2}{\varepsilon^2 Re} + 0.875\frac{l}{D_p}\frac{(1-\varepsilon)}{\varepsilon^2} \tag{22}$$

$$c = \frac{\gamma - 1}{\gamma}\left(\frac{1-\varepsilon}{\varepsilon}\right)\frac{\rho_s c_{ps}T_0(0)}{p_0(0)} \tag{23}$$

$$\begin{aligned} K_c &= \frac{k_{\text{cond}}T_0(0)_q}{l^2Q} \\ K_r &= \frac{16}{3}\sigma\frac{D_p}{l}\frac{qT_0^4(0)}{Ql} \end{aligned} \tag{24}$$

where σ is the Stefan–Boltzmann constant.

In the examples that follow, $T_0(0)$ will generally be set at 300 K, $p_0(0)$ at 100 atm, l and D_p as noted above at 1 cm and 0.5 mm, respectively, ε at 0.3, and k_{cond} at 10 W/mK, which is 0.1 of k_{cond} for graphite.

Parallel-Stream Instability

With this understanding of the magnitudes of the several parameters and their dependence on the operating variables, we can now examine the stability from this relatively simple viewpoint. The dependence of the pressure drop through the

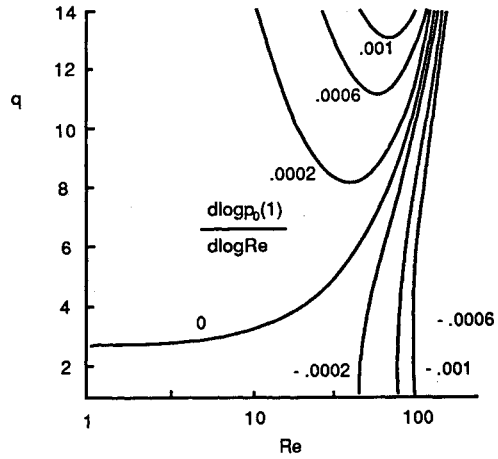

Fig. 2 Stability according to the parallel-stream model, showing contours of constant d log $p_0(1)$/d log Re. In this diagram $p_0(0)$ is held constant at 100 atm. The zero contour is the neutral stability boundary.

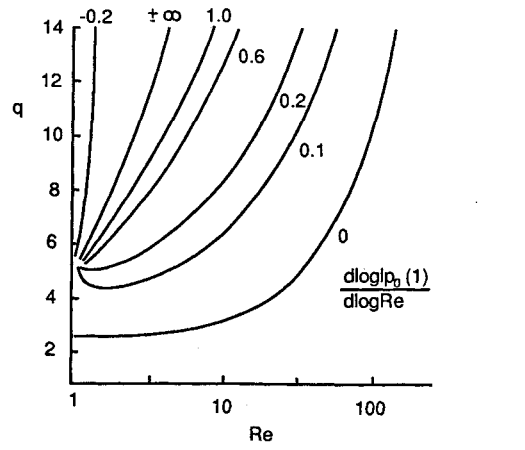

Fig. 3 Stability according to the parallel-stream model, showing contours of constant d log $p_0(1)$/d log Re. In this diagram $p_0(0)$ is taken proportional to the mass flow, to simulate the behavior of a rocket with fixed geometry. The zero contour is the neutral stability boundary.

bed, on the flow parameters, is given by Eq. (11) for $x = 1$. The physically reasonable question is how $p_0(1)$ and q vary with mass flow density for fixed Q and $p_0(0)$. Thus, in Eq. (19) we consider Q fixed and treat q as a function of Re

$$q = \frac{D_p Q l}{c_p T_0(0) \mu_0 Re} \tag{25}$$

since Re is proportional to mass flow density $\rho_0 u_0$.

The local slope $\partial \log p_0(1)/\partial \log Re$ is shown from such a calculation in Fig. 2, as a function of Re and q. The derivative has been taken with Q held constant, and for this example the other parameters are

$l = 0.01$ m
$D_p = 0.5 \times 10^{-3}$ m
$c_p = 1.456 \times 10^4$ J/kg K
$T_0(0) = 300$
$p_0(0) = 10^7$ N/m^2
$\varepsilon = 0.3$
$\nu = 0.7$

For this model, instability is indicated if the slope is positive, i.e., if the pressure at the bed exit boundary increases with increasing Re. Therefore, in the regions where the slope is positive, the flow is unstable, and where it is negative, the flow is stable. The zero contour is the line of neutral stability.

As can be seen from the figure, the flow is indicated to be most unstable for large temperature ratios, $q > 5$, and for $10 < Re < 100$. For $Re > 160$, stability is indicated for all values of q.

These results are entirely consistent with those of Witter,[6] which were obtained under essentially the same assumptions, but by an independent computational scheme called SIMBED. They are also generally consistent with results obtained by Charmchi et al.[5]

In these calculations $p_0(0)$, the inlet pressure to the bed, has been held constant while the mass flow density, represented by Re, and the temperature ratio q, have been varied. In an actual rocket reactor of fixed geometry, if q (i.e., the exit temperature) were held constant while the mass flow was varied, $p_0(0)$ would vary in proportion to the mass flow, since it would be set by a (choked) nozzle throat area, so long as the flow Mach number is small in the frits and bed. Thus, a more realistic representation of the behavior of such a fixed-geometry system is obtained by taking $p_0(0)$ proportional to Re. This has been done in Fig. 3, where $p_0(0) = (10^7$ N/m$^2)(Re/500)$.

The behavior is significantly different from that in Fig. 2 at low Re. Whereas, the flow was indicated to be unstable in the entire low Re high q region in the first case, we now find a stable region for very low Re and high q, where in this case the pressure is low. If this stability model is accepted, it seems unlikely that a system would operate in this region, because it is separated from the normal operating region of high Re and high q by a very unstable region. Furthermore, the primary neutral-stability line is not much different from that for the original case.

In summary, this application of the present model to the parallel-stream instability leads to results consistent with those obtained by other investigators using other modeling techniques, but essentially the same physical assumptions. It suggests a region in Re-q space of high instability, for values of q greater than about four, and for $10 < Re < 200$. For $Re > 200$, it predicts stability. Since the intended operating point of the pebble bed reactor is near $Re = 500$, it should be stable once at full power according to this model. But a startup sequence in which the reactor is brought to operating temperature at low power, then brought to full power at this temperature, would carry the system through a region of potential instability. As we shall see, this same general characteristic is found in the results of the more accurate model.

Complete Instability Model

To capture the zeroth-order variations in x within the bed while at the same time including boundary conditions at the bed inlet and outlet, instability is examined with the introduction of disturbances to the flow quantities. Each of these disturbances is characterized as a Fourier component of a general disturbance, harmonic in $r = (y^2 + x^2)^{1/2}$, exponential in time, but as a function of x to be determined.

Thus, e.g.,

$$p(x, y, z, t) = p(x) e^{i(k_r r) + \omega t} \tag{26}$$

Substituting into Eqs. (14–18) and collecting terms, we find six first-order differential equations for the variables, p, T_g, ρ, u_x, y, T_p, where $y = dT_p/d_x$:

$$\frac{dp}{dx} = -(b_1 T_{g0}^{\nu} + 2b_2) u_x - (b_1 u_0 \nu T_{g0}^{\nu-1}) T_g - (b_2 u_0^2) \rho \tag{27}$$

$$\frac{dT_g}{dx} = H(T_p - T_g) - (\rho_0 \omega) T_g \tag{28}$$

$$\frac{d\rho}{dx} = \left(\frac{1}{T_{g0}}\right)\frac{dp}{dx} - \left(\frac{q}{T_{g0}^2}\right)p - \left(\frac{\rho_0}{T_{g0}}\right)\frac{dT_g}{dx} - \left(\frac{1}{T_{g0}}\frac{d\rho_0}{dx} - \frac{q\rho_0}{T_{g0}^2}\right)T_g \tag{29}$$

$$\frac{du_x}{dx} = -\left(\frac{1}{\rho_0}\frac{d\rho_0}{dx}\right)u_x - \left(\frac{u_0}{\rho_0}\right)\frac{d\rho}{dx} - \left(\frac{1}{\rho_0}\frac{du_0}{dx} + \frac{\omega}{\rho_0}\right)\rho - \left(\frac{k_r^2}{b_2 + b_1 T_{g0}^v}\right)p \tag{30}$$

$$K\frac{dy}{dx} = (Kk_r^2 + c\omega + H)T_p - HT_g + (q\rho_0)u_x + (qu_0)\rho \tag{31}$$

$$\frac{dT_p}{dx} = y \tag{32}$$

The initial conditions are $p(0) = 0$, $T_g(0) = 0$, $\rho(0) = 0$, $y(0) = 0$, and $T_p(0) = 0$, while $u_x(0)$ will be set to unity to scale the disturbance.

These relations now contain the parameters of the zeroth-order solution, and in addition the transverse wave number k_r, and the conductivity K. The growth rate ω is the eigenvalue, to be determined by imposing a boundary condition at the outflow boundary. Since the particle bed is presumed to be bounded both on the inlet side and on the outlet side by plenums, the appropriate outlet condition is $p(1) = 0$.

Approximate Case Neglecting Conduction in x

This is a fairly complex system of equations. In particular, Eqs. (31) and (32), which together constitute a second-order equation for the particle temperature, make the integration time-consuming, because the conductivity K is a small parameter. To simplify the system without losing the qualitative effect of the conduction in the bed, we can neglect the left side of Eq. (31), retaining the term Kk_r^2 on the right side. In this case, Eq. (31) reduces to

$$T_p = \frac{[HT_g - (q\rho_0)u_x - (qu_0)\rho]}{(Kk_r^2 + c\omega + H)} \tag{33}$$

and Eq. (32) is redundant.

It is this simplified case, consisting of Eqs. (27–30) and (33), which has been used to examine the boundary value problem. These five equations have been integrated by a standard fourth-order Runge–Kutta technique, with the initial values $p(0) = 0$, $T_g(0) = 0$, $T_p(0) = 0$, $\rho(0) = 0$, and $u_x(0) = 1$. The procedure used was one that iteratively sought solutions for which $p(1) = 0$, with ω as the iterant. A second iteration then led to identification of the combination of parameters for which $\omega = 0$, the neutral stability boundary.

A typical set of solutions for p, T_g and u_x is shown in Fig. 4. As noted above, they are all scaled by the choice of $u_x(0) = 1$. The small magnitude of the pressure perturbation is a direct result of the low Mach number of the base flow. But we note that the gas temperature perturbation ranges from zero at the inlet to eight times the velocity perturbation, which is nearly constant at unity.

Some discussion of the form of the disturbance may be helpful at this point. From Fig. 4 we see that the velocity normal to the plane of the bed u_x remains nearly constant at the initial value, throughout the bed. The pressure perturbation is negative in the center of the bed, then returns to zero at the exit. The velocity perturbation parallel to the bed

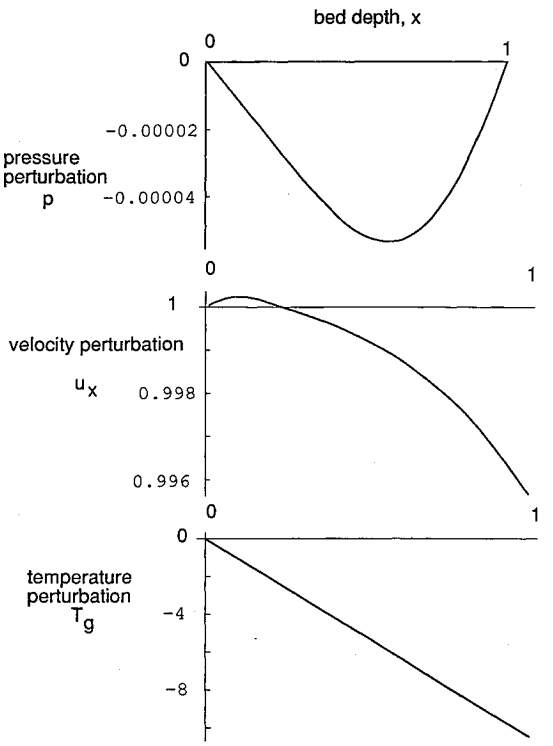

Fig. 4 Typical solutions to the boundary value problem, for the case of $k = 0$. Other parameters are $Re = 100$, $q = 10.5$, $\omega = 0$, and $k_r = 1$.

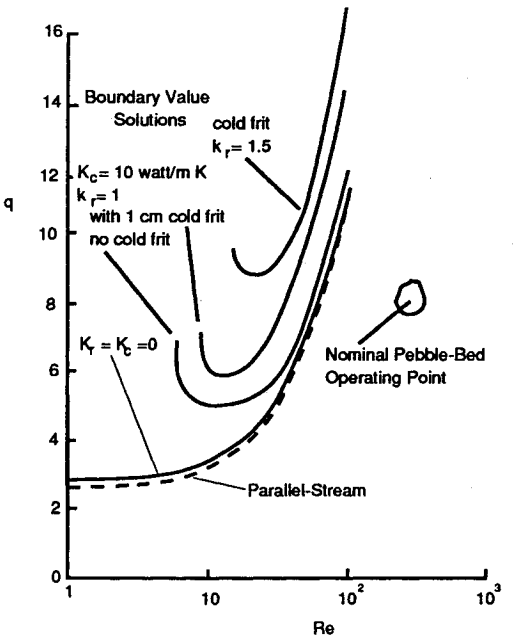

Fig. 5 Neutral stability boundaries from boundary value solutions as exemplified by Fig. 4 compared to that from the parallel-stream model. The boundary value solutions neglect conduction in the x direction, but are otherwise exact.

u_r is proportional to the pressure, and so it is not plotted. It is given by

$$u_r = \left(\frac{-ik_r}{b_1 + T_{g0}^v + b_2}\right)p$$

Thus, u_r is shifted by π in r relative to p, and is opposite in sign. Some reflection leads to the conclusion that throughout the bed the velocity u_r is toward the regions of low pressure

and away from those of high pressure. This of course represents the flow redistribution along the bed, which is ruled out in the parallel-stream model.

The temperature disturbance increases negatively throughout the bed, providing an increase in density, which in turn leads to an increase in local mass flow density, even though the pressure has dropped in the center of the bed. This increase in mass flow density must be present for consistency with the mass flow toward the low-pressure region represented by u_r.

Neutral stability boundaries found from this model are shown in Fig. 5 for two assumptions about the heat transfer, along with that for the parallel-stream model (and results on the effect of frits that will be discussed later). There is remarkable similarity in the results of the parallel-stream and boundary value models, when heat conduction is neglected.

On the other hand when a realistic amount of heat conduction is included, the boundary value model predicts a considerably smaller region of instability than that predicted by the parallel-stream model. Thus one can reasonably conclude that the parallel-stream model is not adequate at low *Re*.

Effect of Cold and Hot Frits

The above calculation is readily extended to include the effects of frits, since the governing equations for the flow in the frit are similar to those in the bed, with $Q = 0$. The matching conditions at the frit–bed interface are simply that all the flow variables, ω and k_r are continuous. The eigen value is still determined by the condition that $p = 0$ at the bed exit.

Calculations have been carried out for an example in which the cold frit has the same geometrical properties as the bed, i.e., a thickness of 1 cm and a particle size of 0.5 mm. Thus, it differs from the bed only in having no heat addition. Certainly this is not a typical frit design. It is meant only to show the effect of the cold frit. This can be seen from Fig. 5, where the line marked "with 1 cm cold frit" represents this case. It is to be compared to the case marked "no cold frit."

We see that the effect of the cold frit is stabilizing. There is no doubt that a frit with a larger pressure drop would have a larger stabilizing effect.

The effects of both cold and hot frits have been calculated by the second author using the same approach described above, but with a completely independent analysis and computational procedure. Figure 6 shows the same results as Fig. 5 where they overlap. In addition, it shows the effect of a hot frit, which is to destabilize the bed slightly for high *Re*, but to stabilize it for low *Re*. This result is not available from the parallel-stream approach, and could be of importance for low-power operation at high-temperature ratios.

From these results we can conclude that whereas the bed by itself is subject to instability, it probably can be stabilized by a cold frit under most circumstances. The effect of the hot frit is somewhat more complex than might be thought intuitively. The model presented here provides a quantitative means for the design of both cold and hot frits.

Modeling for Fixed Geometry

The results in Figs. 5 and 6 are all for the standard conditions described in the section Parameters. In particular, as noted in the discussion of the parallel-stream model, the inlet pressure has been set at 100 atm (Fig. 6 is for 60 atm rather than 100). Thus, these figures, in principle, cannot be interpreted as the stability behavior of a system of fixed geometry, when the mass flow is varied. As noted there, for such a fixed geometry, the inlet pressure to the bed would be proportional to mass flow (or *Re*) for fixed exit temperature. To approximate this situation we might put $p_0(0) = (10^7\ \mathrm{N/m^2})(Re/500)$. But sample calculations with this change show that the change in the stability boundary is, in fact, very small. From Eqs. (19–24) we can see that the reason is the absolute pressure level enters only in the magnitude of the conductivity ratio c, given by Eq. (23). At the pressure levels of practical interest, the particle heat capacity dominates the gas heat capacity, so

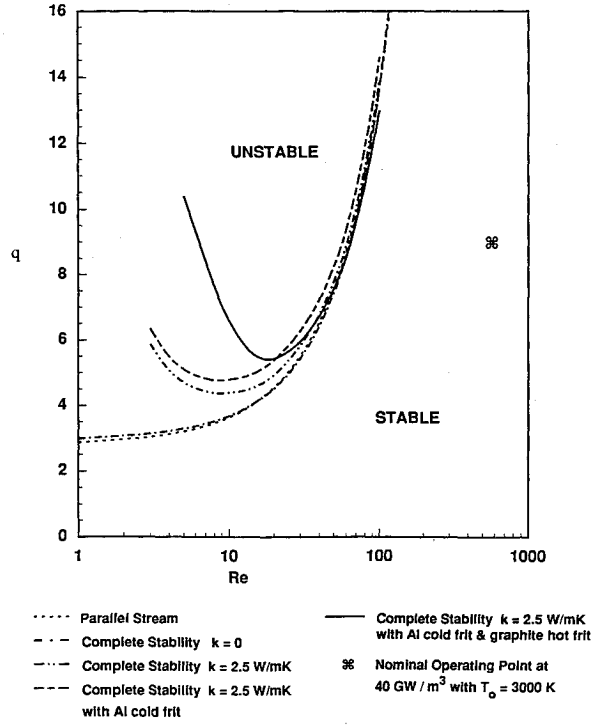

Fig. 6 Stability boundaries computed by an independent procedure, showing agreement with Fig. 5. These results also include the effect of a hot frit, which is shown to be slightly destabilizing for high *Re*, but stabilizing for low *Re*.

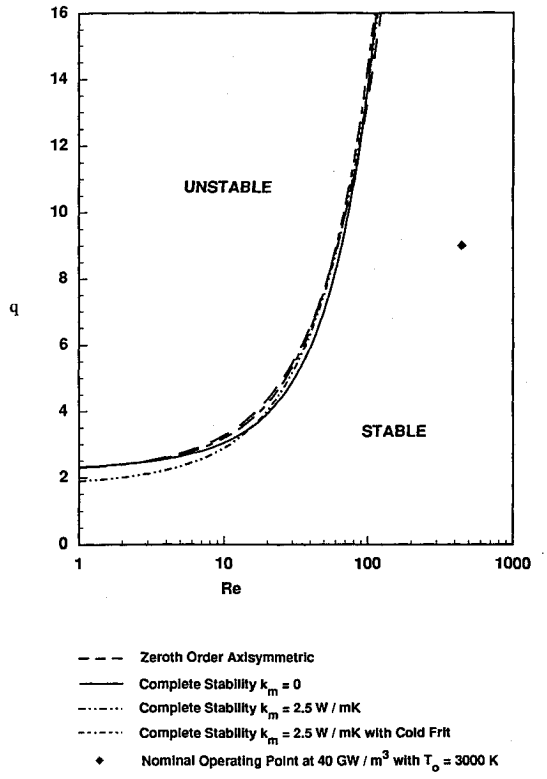

Fig. 7 Stability boundaries for annular geometry. The particle bed has inner radius of 3.35 cm and outer radius of 4.35 cm. The outer radius of the cold frit is 4.5 cm and the inner radius of the hot frit is 3.05 cm. Flow is radially inward.

that a change in pressure has little effect over most of the operating range.

Effect of Annular Geometry

All of the above discussion has been under the assumption that the geometry of the bed is plane–parallel. In fact, the geometries of interest for the nuclear rocket are annular, with flow inward through first a cold frit, then the particle bed, and finally a hot frit. The flow would then exit along the bore of the hot frit. The effects of this overall geometry on the mean flow have been addressed by others. In the spirit of the present discussion we may ask how the annular geometry and the associated radial inward flow change the stability.

To answer this question, the second author has generalized the above approach to the annular geometry. This extension is straightforward, and so the analysis will not be presented here. The results are presented in Fig. 7, in the same format as Fig. 6. It is necessary in this case to specify the radii of the particle bed and of the frits; these are given in the figure caption.

Comparison of these two figures shows the following:

1) For the assumptions of either the parallel-stream model or the complete stability model neglecting heat conduction in the bed, the predicted stability boundaries are virtually identical for the annular and plane-parallel geometries.

2) For the annular geometry, the cold frit does not have the stabilizing influence at low Re and high q that it has for the plane–parallel geometry.

Conclusions

Comparison of two quite different approaches to modeling the stability of the particle-bed reactor, all with consistent physical assumptions, shows that a complete linear stability model such as that presented here is, in fact, necessary for reliable prediction of the stability of the particle-bed reactor. The approach, termed here the parallel-stream model, where the reactor is assumed to be composed of a series of channels coupled only at their inlets and outlets, does not accurately represent the stability at low Re, nor does it represent the effects of heat conduction in the bed or of inlet and outlet frits. The model termed here the complete model (in the limited context of this study) should be capable of accurately representing the effects of the cold and hot frits, and of heat conduction and radiation in the particle bed.

From the sample calculations that have been carried out, it can be concluded that a particle bed without a cold frit would be subject to instability if operated at the high temperatures desired for nuclear rockets, and at power densities below about 4 MW/l. Since the desired power density is about 40 MW/l, it can be concluded that operation at design exit temperature, but at reduced power, could be hazardous for such a reactor.

The calculations for plane–parallel bed geometry suggest that appropriate cold and hot frits could cure the instability, but extension of the analysis to the annular geometry preferred for a reactor indicates that this stabilizing effect may not be present for the annular geometry. More definite conclusions must await calculations for specific designs.

Acknowledgments

This research was supported by the Space Nuclear Propulsion Office of NASA Lewis Research Center. The authors wish to acknowledge helpful discussions with Frank E. Marble, and with David Suzuki, Timothy Lawrence, and Jonathan Witter.

References

[1]Bussard, R. W., and DeLauer, R. D., *Nuclear Rocket Propulsion*, McGraw–Hill, New York, 1958, pp. 129–133.

[2]Bussard, R. W., and DeLauer, R. D., *Fundamentals of Nuclear Flight*, McGraw–Hill, New York, 1965, pp. 137–149.

[3]Reshotko, E., "An Analysis of the Laminar Instability Problem in Gas-Cooled Nuclear Reactor Passages," *AIAA Journal*, Vol. 5, No. 9, 1967, pp. 1606–1615.

[4]Bankston, C. A., "The Transition From Turbulent to Laminar Gas Flow in a Heated Pipe," *Journal of Heat Transfer*, Vol. 92, Nov. 1970, pp. 569–579.

[5]Charmchi, M., McKelliget, J. W., Rand, M., and Maise, G., "Thermo-Hydraulic Characteristics of Gas-Cooled Particle Bed Reactors," *Proceedings of the 4th International Topical Meeting on Nuclear Reactor Thermal-Hydraulics (NURETH-IV)*, G. Braun, Karlsruhe, Germany, Vol. 1, 1989, pp. 139–145.

[6]Witter, J. K., Lanning, D. D., and Meyer, J. E., "Flow Stability Analysis of a Particle-Bed Reactor Fuel Element," personal communication, Massachusetts Inst. of Technology, Cambridge, MA, Oct. 1992.

[7]Ergun, S., "Fluid Flow Through Packed Columns," *Chemical Engineering Progress*, Vol. 48, No. 2, 1952, pp. 89–94.

[8]Zel'dovich, Y. B., and Raizer, Y. P., *Physics of Shock Waves and High-Temperature Hydrodynamic Phenomena*, Academic, London, 1966.